

Fermi National Accelerator Laboratory

TM-1510

Space-charge Effects in the Main Ring at 8 GeV

S. R. Mane

Fermi National Accelerator Laboratory
P.O. Box 500, Batavia, Illinois 60510

January 1988



Operated by Universities Research Association Inc. under contract with the United States Department of Energy

Space-charge Effects in the Main Ring at 8 GeV

S.R. Mane

Fermi National Accelerator Laboratory, P.O. Box 500, Batavia, Il. 60510

I. INTRODUCTION

This is a note on the effects of space-charge on particle behavior in the Main Ring. At first, to elucidate various basic points, an idealized model of the Main Ring was studied. Then the TEVLAT program was used, with a sample Main Ring lattice.¹ The TEVLAT program was modified to include space-charge kicks. The idealized model mentioned above consisted of linear dynamics with localized nonlinear elements (thin sextupoles). The incoherent space-charge force was included as a series of kicks applied uniformly around the ring (because the space-charge force is not localized). The space-charge force changes the tune and the oscillation amplitude (action variable) of a particle. However, the effect of this was not fed back into the beam emittance (and thus the change to the space-charge force itself).² Finally, synchrotron oscillations were included, and some brief results are presented.

II. ACCELERATOR MODEL

The Main Ring has a mean radius of $R = 1000$ m, with six superperiods (neglecting the vertical overpasses). The horizontal and vertical tunes are $Q_x = 19.42$ and $Q_y = 19.37$ respectively, and the beta functions vary between 30 to 100 m. The average beta function is taken to be $\bar{\beta}_x = \bar{\beta}_y = 50$ m in this note. The harmonic number is $h = 1113$, and the total number of particles in the ring is taken to be $N = 2 \times 10^{13}$ in 1113 bunches. A bunching factor of $B = 0.1$ is assumed, which gives an r.m.s. bunch length (one standard deviation) of $\sigma_z = 0.225$ m, which is much larger than the transverse sizes σ_x and σ_y , as will now be shown.

The beam sizes are calculated as follows. In this note, the value used for the normalized transverse emittances is $\epsilon_{Nx} = \epsilon_{Ny} = \epsilon_N = 10\pi$ mm-mrad, where the figures refer to 95%

of the beam. This is related to the r.m.s. unnormalized beam emittances via $\epsilon_{x,y} = \epsilon_{N_x, N_y} / (6\pi\beta\gamma)$. The average r.m.s. beam sizes around the ring are given by

$$\sigma_x = \left[\bar{\beta}_x \epsilon_x + \overline{(\eta \Delta p/p)^2} \right]^{1/2}, \quad \sigma_y = [\bar{\beta}_y \epsilon_y]^{1/2}, \quad (1)$$

where overhead bars denote average values around the ring. All the results presented here are at 8 GeV kinetic energy, so $\gamma = 8.938/.938 = 9.53$ and $\beta = 0.994$. Here η denotes the horizontal dispersion and $\Delta p/p$ denotes the momentum spread. In this note, the values used are $\overline{\eta^2} = 9 \text{ m}^2$ and $\Delta p/p = 10^{-3}$. Then, using the values quoted above for $\bar{\beta}_x$, etc., $\sigma_x = 4.22 \text{ mm}$ and $\sigma_y = 2.97 \text{ mm}$, which are seen to be much less than σ_x .

A simplified accelerator model was used to obtain the results presented in the next few Sections. The model consisted of a set of $N_{cell}(= 100)$ identical cells. The dynamics was linear in each cell, with a phase advance of $2\pi Q_{x,y}/N_{cell}$. There was no transverse coupling. The space-charge force was represented by kicks applied between cells, hence there were N_{cell} kicks. A simplified model of the space-charge electric field was used, valid for round beams. This is approximately valid if the horizontal and vertical beam sizes are not significantly different. For a round Gaussian beam of line charge density λ and size σ , the electric field points radially outwards from the beam center and is given by

$$E(r) = \frac{2\lambda}{r} (1 - e^{-r^2/2\sigma^2}), \quad (2)$$

where $r = \sqrt{x^2 + y^2}$.

The space-charge force is of course directed outwards from the beam centroid. The centroid does not necessarily lie on the accelerator closed orbit. This complicates the calculation of the space-charge force. In this note the beam will be assumed to be a Gaussian in all planes, and centered on the closed orbit, to simplify the calculation. This is a reasonable approximation if the transverse beam size is much larger than the displacement of the beam centroid from the closed orbit.

Additional nonlinearities, such as sextupoles, were also described by kicks. To begin with, the only nonlinearity used was the space-charge force.

III. RESULTS

A. TUNE vs. AMPLITUDE

A particle was tracked through the above model, with different starting conditions, to measure the space-charge tune shift. The only nonlinearity in the motion was the space-charge force. The results are shown in Fig. 1. For the solid curves, the starting condition was $x \neq 0$, $x' = y = y' = 0$ for the horizontal tune, and $y \neq 0$, $x = x' = y' = 0$ for the vertical tune. For the dashed curves, the starting condition was $x = y(\neq 0)$, $x' = y' = 0$. As expected, the tunes shifts are negative, and larger in magnitude for small amplitudes. Note also that, apart from very small and very large amplitudes, the dependence of the tunes on the trajectory is affected by the transverse coupling of the space-charge force. The dashed curves approach the linear lattice values of $Q_x = 19.42$ and $Q_y = 19.37$ more rapidly. The Laslett formula for the linear tune shift is

$$\Delta Q_x = -\frac{\tau_p N R \bar{\beta}_x}{\pi \beta^2 \gamma^3 \sigma_x (\sigma_x + \sigma_y) \sqrt{2\pi \sigma_x}}, \quad (3)$$

with $x \leftrightarrow y$ for ΔQ_y . For the above model, Eq. (3) predicts $\Delta Q_x = -0.094$ and $\Delta Q_y = -0.134$. Note that the Laslett formula is derived assuming uncoupled motion, and so should be compared with the results from the solid curves in Fig. 1, which are $\Delta Q_x = -0.093$ and $\Delta Q_y = -0.133$, which agree closely with Eq. (3). The linear tune shifts from the dashed curves in Fig. 1 are slightly larger ($\Delta Q_x = -0.1$ and $\Delta Q_y = -0.145$), but the agreement is still good.

B. SMEAR

It is reported in Ref. 2 that the space-charge force results in some smear, but that this is mainly due to its effect on transverse coupling, and not to its nonlinear nature. This was checked, and similar conclusions were obtained. A particle was tracked through the lattice with the starting condition (i) $x \neq 0$, $x' = y = y' = 0$ (no $x - y$ coupling), and (ii) $x = y \neq 0$, $x' = y' = 0$. The particle coordinates $\{x_1, x_2\} = \{x, \alpha x + \beta x'\}$ were measured at $\theta = 0, 2\pi, 4\pi$, etc. The results are shown in Fig. 2a (case (i) — no coupling), and Fig. 2b (case (ii) — transverse coupling), for initial starting amplitudes of $\frac{1}{2}\sigma_x$, σ_x , $\frac{3}{2}\sigma_x$, and $2\sigma_x$. There is distinct smear in Fig. 2b, but almost none in Fig. 2a, in agreement with

the findings in Ref. 1.

C. SPACE-CHARGE AND ONE SEXTUPOLE

Up to now, the only nonlinearity in the model has been the space-charge force. It causes amplitude-dependent tune shifts (hence a tune spread in the beam), but does not lead to unbounded orbits. The phase space is stable. Other nonlinearities in the ring, however, such as a sextupole, do excite resonances, leading to unbounded orbits, and a finite dynamic aperture. We might expect that because the space-charge induces amplitude-dependent tune shifts, it might change the dynamic aperture produced by these other nonlinearities. In this section, we include one sextupole in the ring, at $\theta = 0$, and examine the effect of space-charge on the dynamic aperture due to this sextupole.

First, particles were tracked around the ring with only the sextupole and no space-charge, and then space-charge was included. Recall that the linear lattice tunes were $Q_x = 19.42$ and $Q_y = 19.37$. The sextupole strength was defined as

$$s_x = \frac{L}{2B\rho} \frac{d^2 B}{dx^2}, \quad (5)$$

which produces a deflection

$$\Delta x' = s_x(x^2 - y^2), \quad \Delta y' = 2s_x xy. \quad (6)$$

To avoid unnecessary complications, only horizontal motion was treated. The results are shown in Fig. 3, for $s_x = 1 \text{ m}^{-2}$. In Fig. 3a, there was no space-charge force. In Fig. 3b, there was both space-charge and the sextupole. There was no tune modulation. The apparently stochastic or chaotic nature of some of the trajectories is simply because the particles were not tracked for long enough to produce smooth curves in all cases. The central part of Fig. 3b is shown on a larger scale in Fig. 4. In Fig. 3a, the small-amplitude (linear) tune is 19.42, and decreases to 19.33 as the amplitude of oscillation increases. The five islands corresponding to $Q_x = 19.4$ are clearly visible. In Fig. 3b, the space-charge reduces the tune at small amplitudes, whereas the sextupole reduces the tune at large amplitudes, hence the tune starts off at a low value, increases with amplitude, then decreases as the the effect of the space-charge weakens and that of the sextupole

dominates. The small-amplitude tune is below 19.33, because the linear tune is 19.42 and the space-charge linear tune shift is approximately -0.1 . The tune increases with amplitude, and crosses the resonant value of 19.33, and three resonance islands appear, which are bounded by stable trajectories. Note that such islands did not appear in Fig. 2a (space-charge only, no sextupole). The tune continues to increase, but does not reach 19.4 (no islands corresponding to this resonance appear). The tune then decreases to 19.33 again, and unbounded orbits appear, as in Fig. 3a. The dynamic aperture is slightly smaller than in Fig. 3a.

D. SPACE-CHARGE AND MANY SEXTUPOLES

The above calculation was illustrative only. The sextupole strength was much stronger than in a realistic lattice (and there was only one sextupole), in order to exaggerate the effects of nonlinearities on the structure of the phase-space. Now let us consider a distribution of sextupoles in the ring, with values similar to those in the Main Ring. One sextupole per FODO cell was used. All sextupoles had the same strength. Again, only horizontal motion was treated. The results are shown in Fig. 5, using the same format as in Fig. 3. The results in Fig. 5a were obtained with only sextupoles, and in Fig. 5b space-charge was included. The sextupole strength used was $s_x = 0.03 \text{ m}^{-2}$. The space-charge makes almost no difference to the shapes of the phase-space trajectories. The trajectories are almost, but not exactly, circles. This can be seen more clearly in Fig. 6, where the data in Fig. 5 is shown in a graph of I vs. ψ , where

$$I = x_1^2 + x_2^2 = x^2 + (\alpha_x x + \beta_x x')^2, \quad \psi = -\tan^{-1}\left(\frac{x_2}{x_1}\right) \quad (7)$$

are the linear action-angle variables. The crosses (circles) refer to data calculated with (without) space-charge. Perfectly circular phase-space trajectories in Fig. 5 would yield horizontal straight lines in Fig. 6. The action variable is almost the same with and without space-charge. The tunes are of course different. This can be seen in Fig. 7, where the fractional parts of the tunes of the trajectories in Figs. 5 and 6 are shown as a function of initial amplitude. Once again the crosses (circles) refer to data calculated with (without) space-charge. The curves through the data points were obtained using a polynomial curve

fitting program.

E. MAIN RING

The above results were obtained using an idealized model with sextupoles as the only nonlinearities. The program TEVLAT was now used to study the Main Ring. The program was modified to include the space-charge force. Each multipole kick in TEVLAT was followed by a space-charge kick, using the same model for the space-charge force as above. The same values were used for the number of particles, bunching factor, etc.

A Main Ring lattice with linear tunes of $Q_x = 19.42$ and $Q_y = 19.38$ was used.¹ The lattice included vertical overpasses, harmonic and chromaticity correction sextupoles, and systematic sextupole and decupole moments in the dipoles. It had no octupoles and no random fields.

As before, graphs were made of the orbital tune vs. amplitude, and phase-space plots of the trajectories at $\theta = 0$. Figs. 8 and 9 show the fractional horizontal and vertical tunes, respectively, as a function of starting amplitude for particles launched with $x \neq 0$, $y = 0$ (Fig. 8), and $y \neq 0$, $x = 0$ (Fig. 9). In both cases $x' = y' = 0$ initially. The crosses (circles) refer to data calculated with (without) space-charge. For starting amplitudes $y > 12$ mm, the particles were lost from the ring. The small-amplitude tune shifts are in agreement with the Laslett formula. The horizontal tune decreases with amplitude at large amplitudes because of the effect of the magnet nonlinearities.

Figs. 10a and 10b are plots of the trajectories in horizontal phase-space at $\theta = 0$, without and with space-charge, respectively. In both cases the starting condition was $x \neq 0$, $x' = y = y' = 0$. We see that there is some difference in the phase-space structure, because of the space-charge tune shift. Five resonance islands appear when the fractional part of the tune crosses the value of 0.4 in Fig. 10b. In Fig. 11, the same data are plotted in a graph of I vs. ψ . The crosses (circles) again refer to data calculated with (without) space-charge. We see that the space-charge force makes little difference to the oscillation amplitudes (action variables), even though it does produce resonance islands that would otherwise be absent.

F. SYNCHROTRON OSCILLATIONS

The above results did not include synchrotron oscillations. The latter can cause tune modulation, causing a particle to cross resonances in transverse phase-space,

$$Q_n = Q_0 + \delta Q \sin(2\pi Q_n n) \quad (8)$$

where Q_n is the tune (horizontal or vertical) at the start of the n^{th} turn, and δQ is the amplitude of the tune modulation in that plane. It can also change the strength of the space-charge force, because $\sigma_{x,y}$ depend on the longitudinal position z :

$$\sigma_{x,y} = \sigma_{x0,y0} \exp\left(-\frac{z^2}{2\sigma_z^2}\right). \quad (9)$$

A particle was tracked around the Main Ring using TEVLAT and the lattice mentioned above. TEVLAT does not calculate the longitudinal position z , hence the graphs below only include the effects of tune modulation by the synchrotron oscillations. A momentum offset of $\Delta p/p = 5 \times 10^{-4}$ was used. The starting amplitude was $x = 15$ mm. Once again, only horizontal motion was treated, and the results are shown in Fig. 12. The crosses (circles) refer to data calculated with (without) space-charge. The displacement of the closed orbit due to the momentum offset induced by the synchrotron oscillations has been subtracted in plotting Fig. 12. We see that space-charge again makes little difference to the results.

Note that the data in Fig. 12 span only a few synchrotron periods. The point being made is it not to examine the particle behavior over many synchrotron periods, but rather to compare the difference in the particle behavior with and without space-charge.

IV. CONCLUSION

It appears that space charge makes little difference to particle behavior in the Main Ring at 8 GeV, except for tune-shifts. This conclusion has been reached by comparing results obtained by tracking with and without space-charge. Two models were used, a Main Ring lattice and an idealized model, described in Section II. More detailed studies, especially with synchrotron oscillations, need to be performed to make the above conclusion more definite. In particular, the absence of random fields in the Main Ring lattice meant

that the driving terms of resonances such as $Q_x = 19.33$ or $Q_x = 19.4$ were very weak. Thus a more realistic lattice needs to be used.

ACKNOWLEDGEMENTS

The author thanks D. Edwards for supervising this work. He also thanks R. Gerig for help with the TEVLAT program and for supplying sample Main Ring lattice datafiles, and C. Ankenbrandt, G.P. Jackson and S. Stahl for helpful comments and references. This work was supported by the Universities Research Association Inc., under contract from the U.S. Department of Energy.

References

- 1 The version of TEVLAT and the Main Ring lattice used were obtained from R. Gerig.
- 2 Many of the ideas here follow the work of M. Furman, SSC-115 (1987) (unpublished), and presented at the IEEE Particle Accelerator Conference, Washington D.C. (1987).

Fig 1

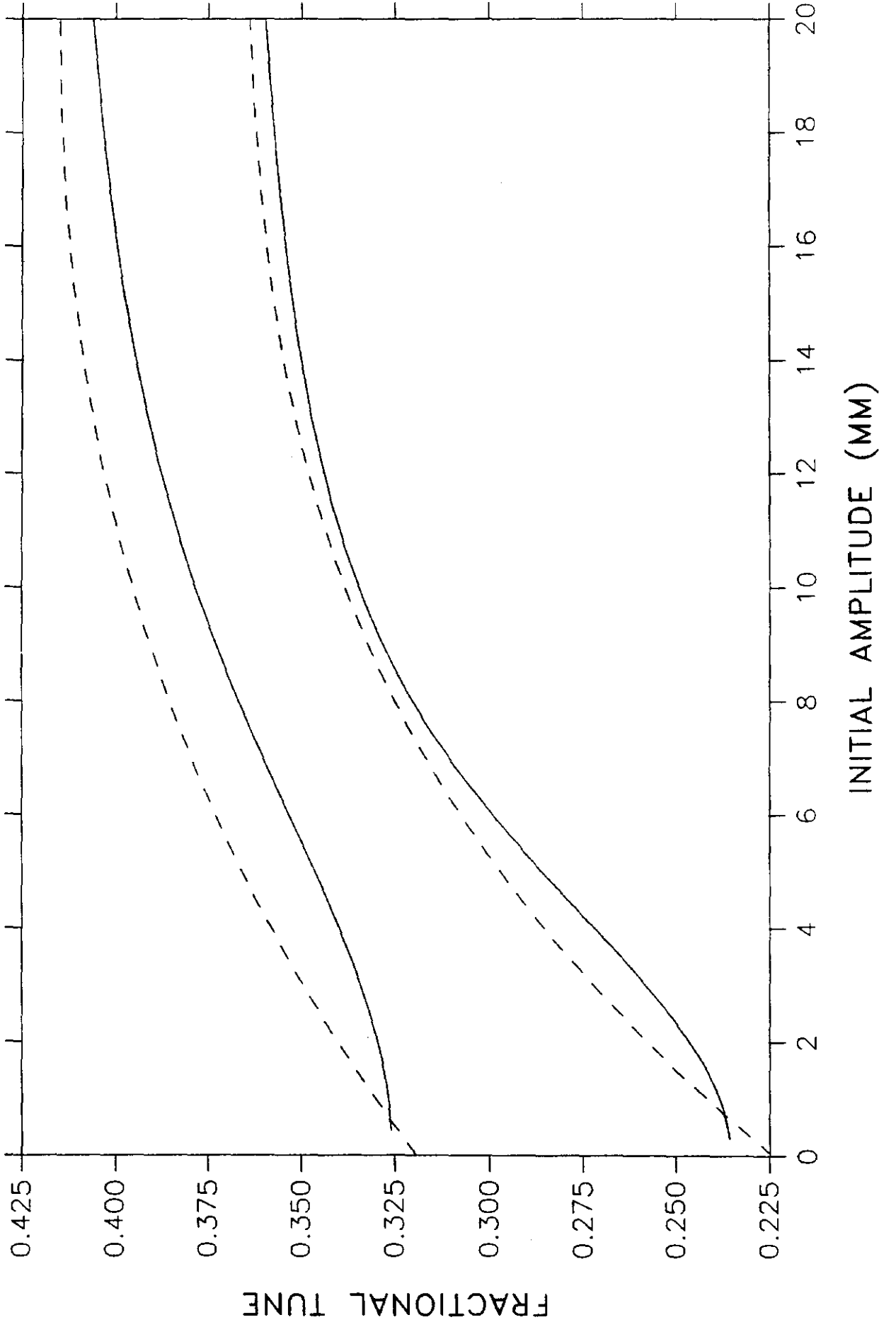
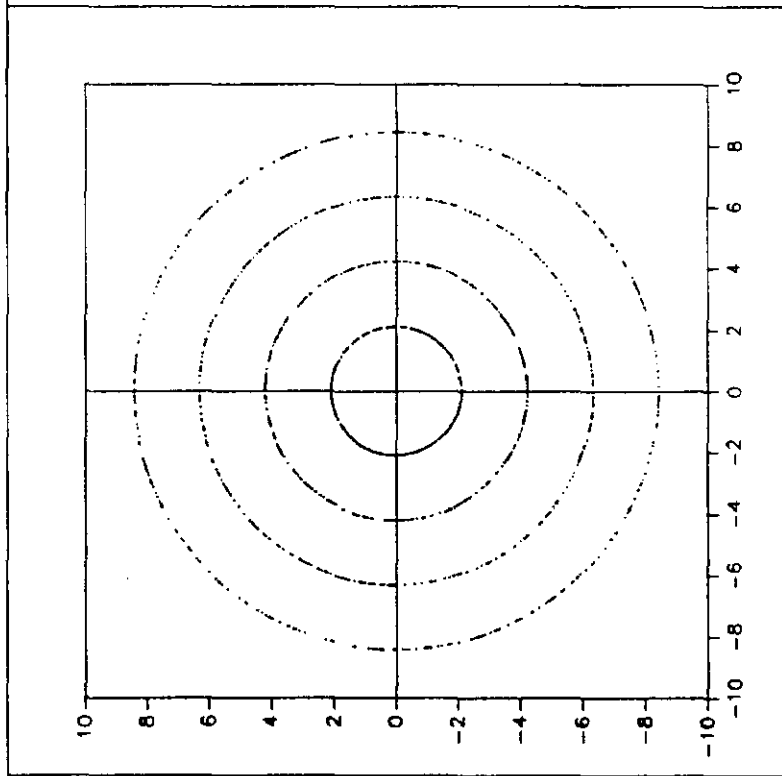


Fig 2

(a)



(b)

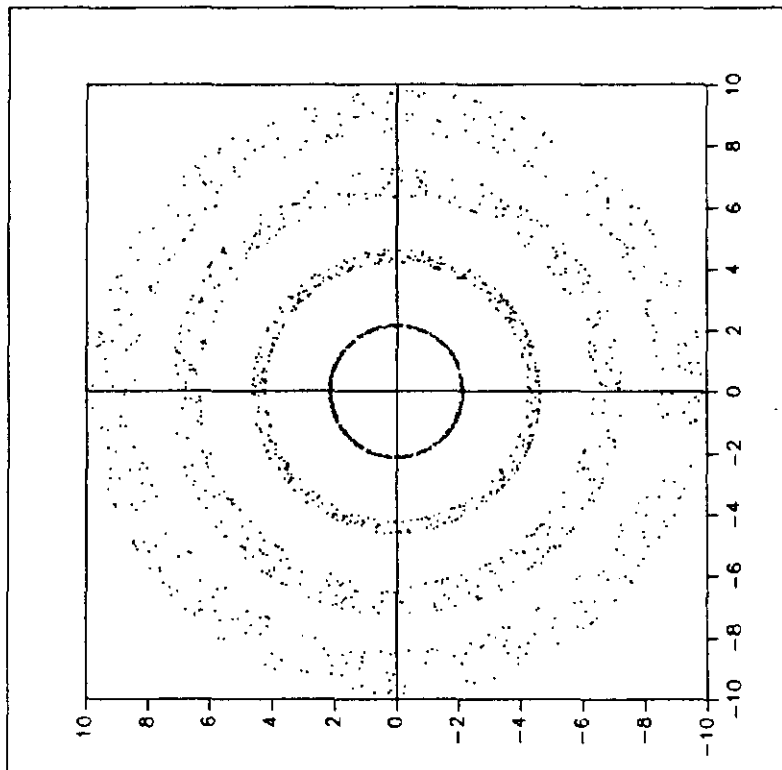
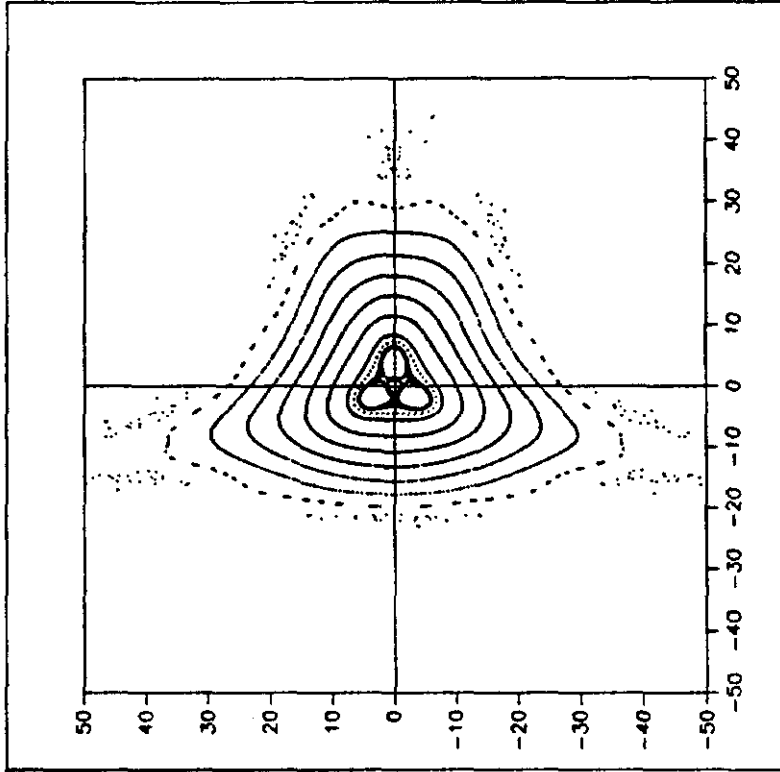


Fig 3

(b)



(a)

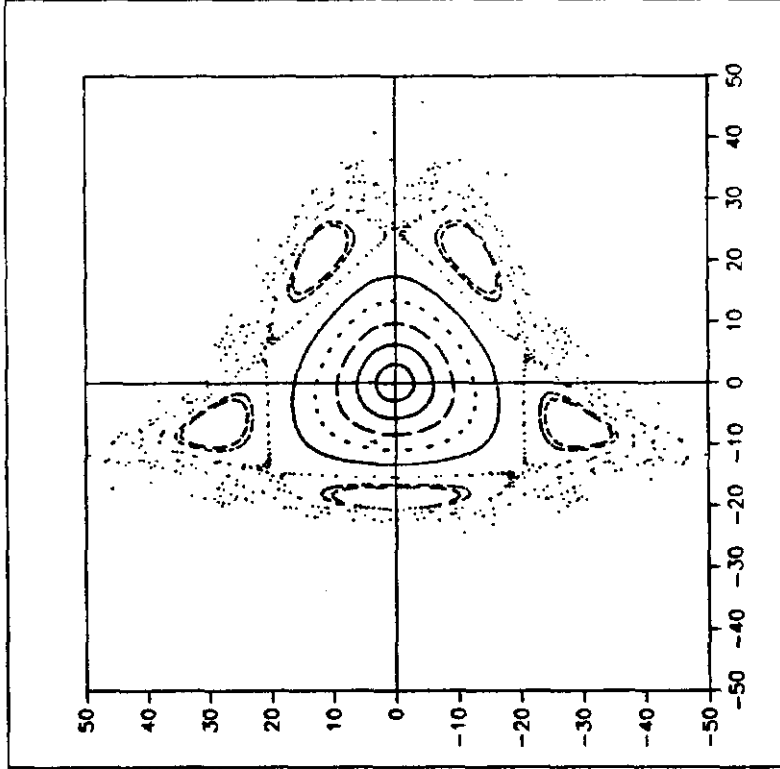


Fig 4

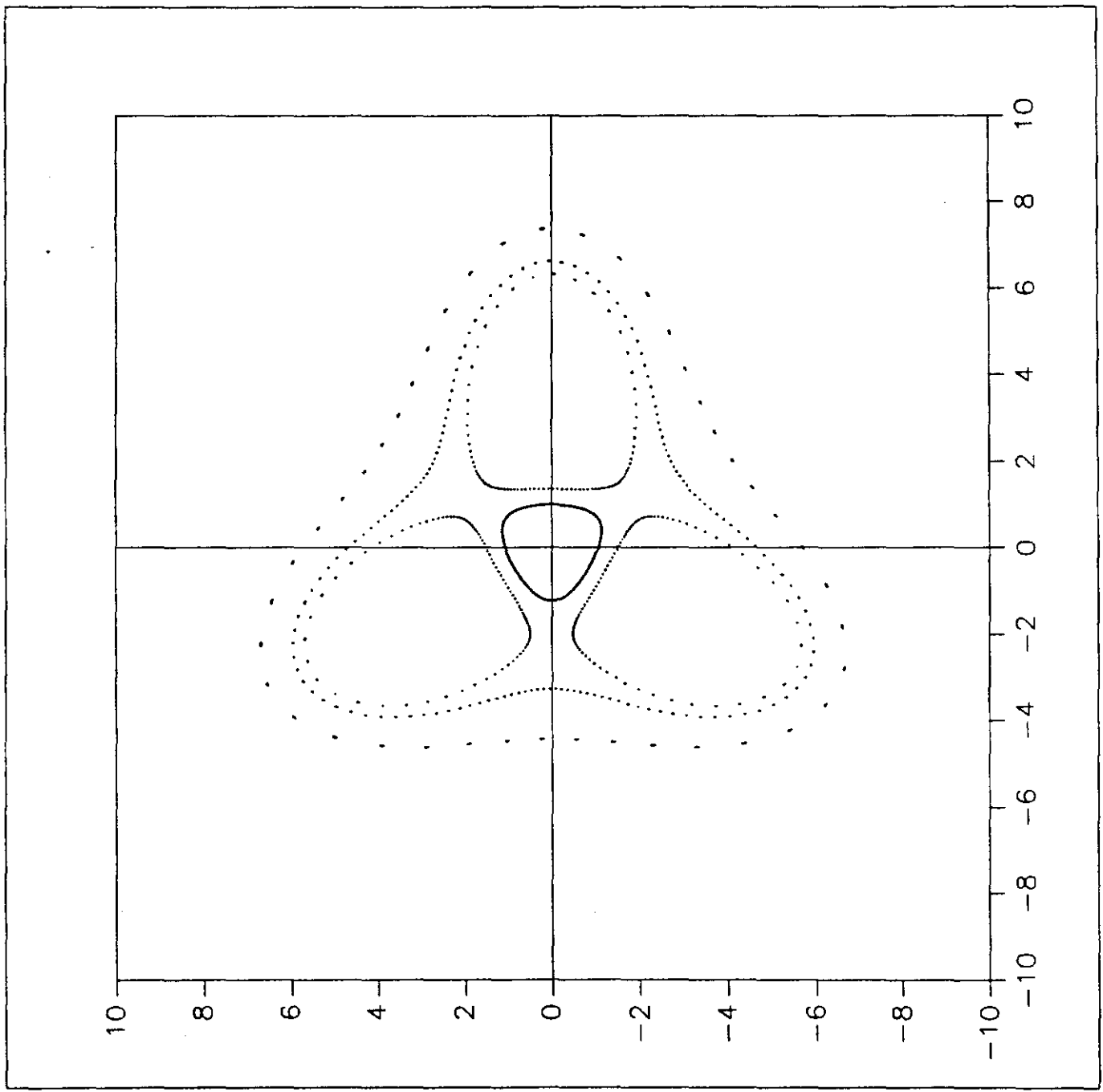
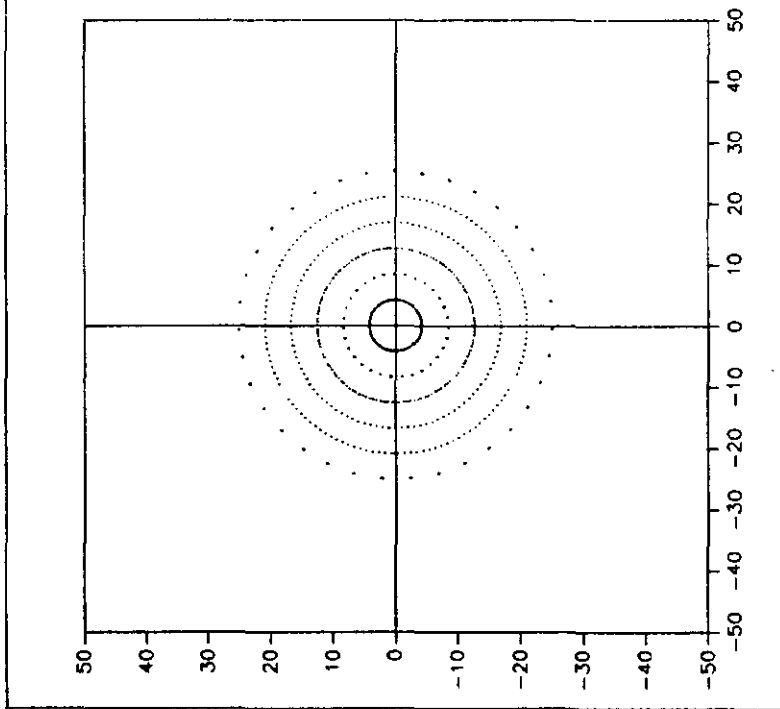


Fig 5

(a)



(b)

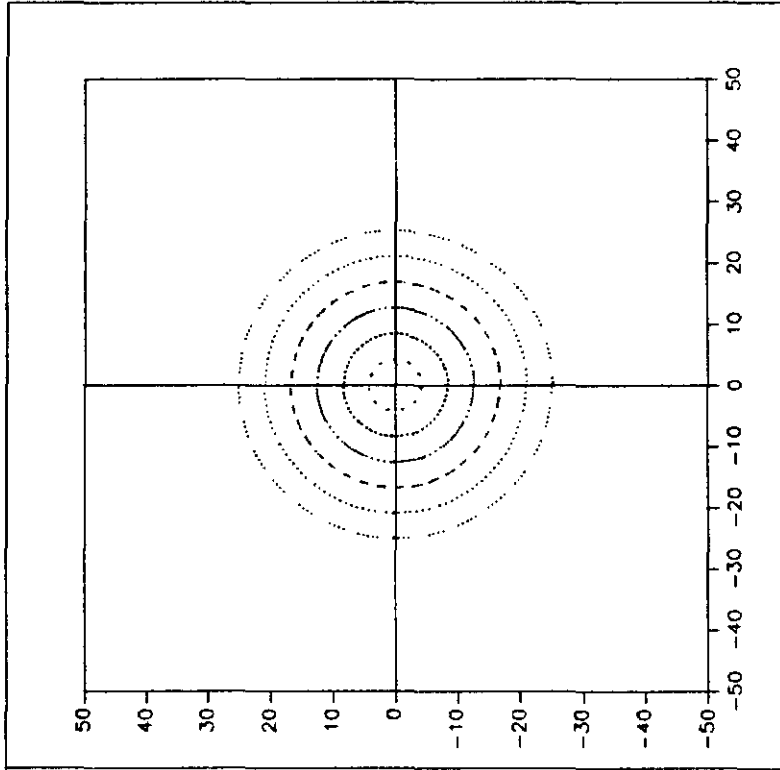


Fig 6

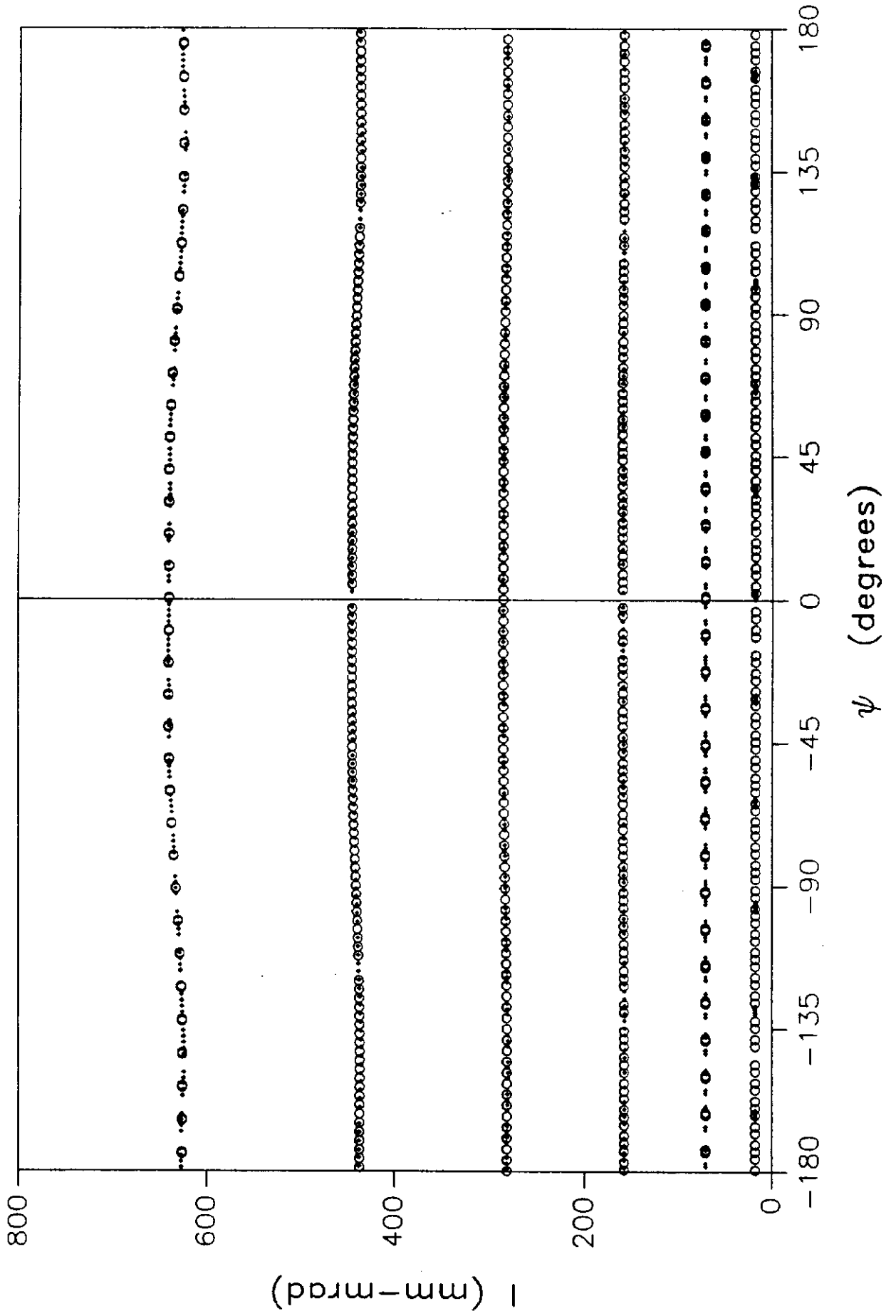


Fig 7

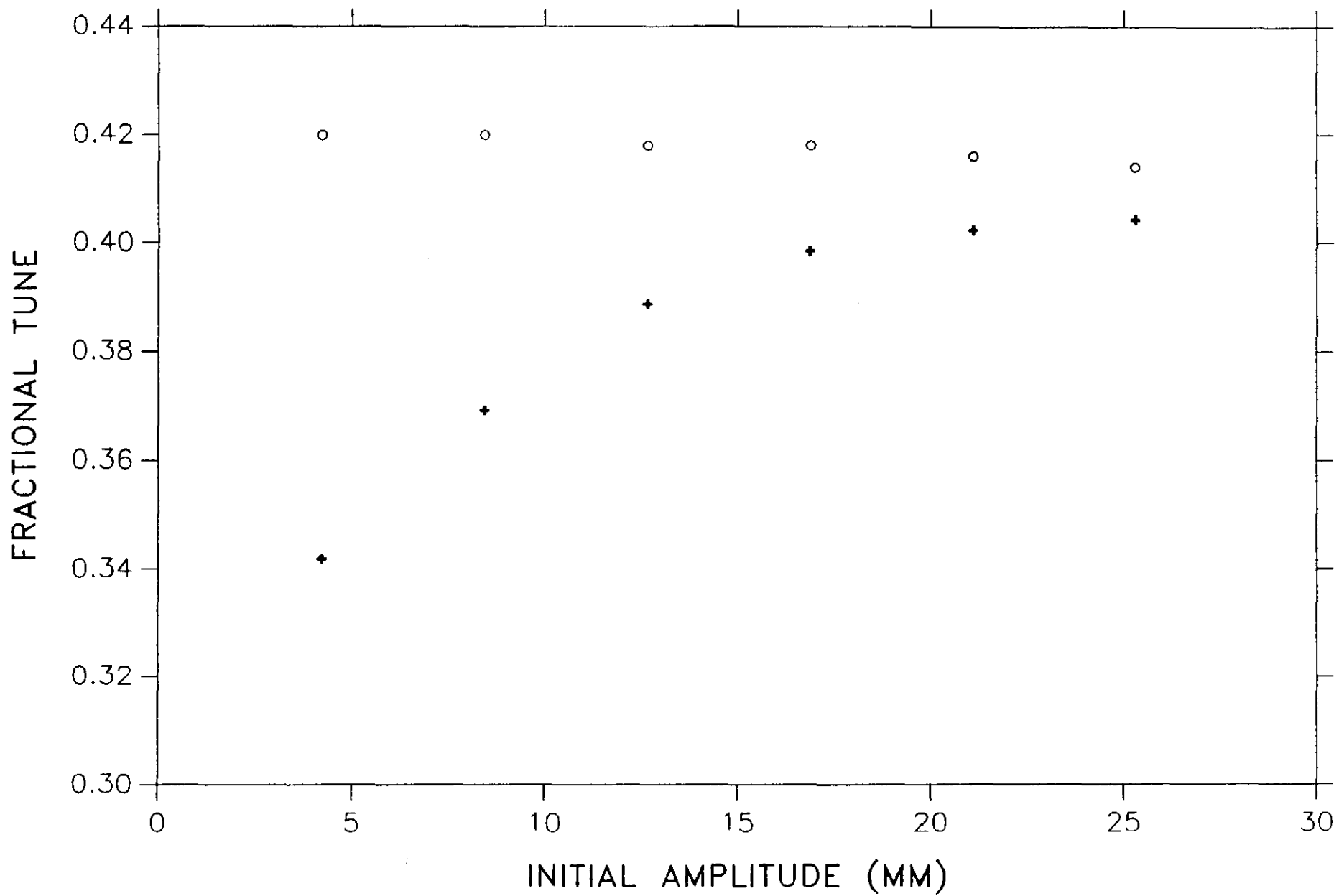


Fig 8

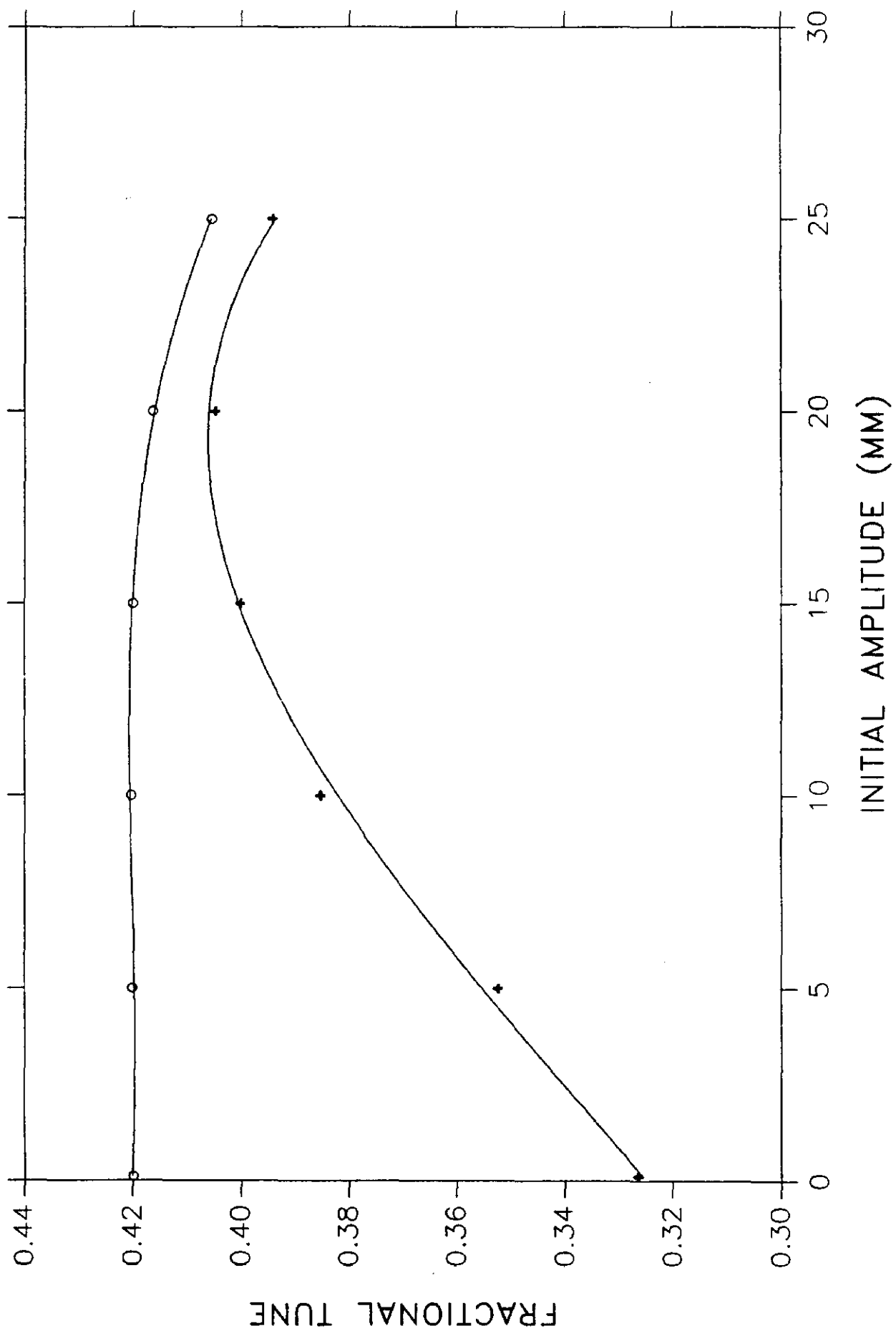


Fig 9

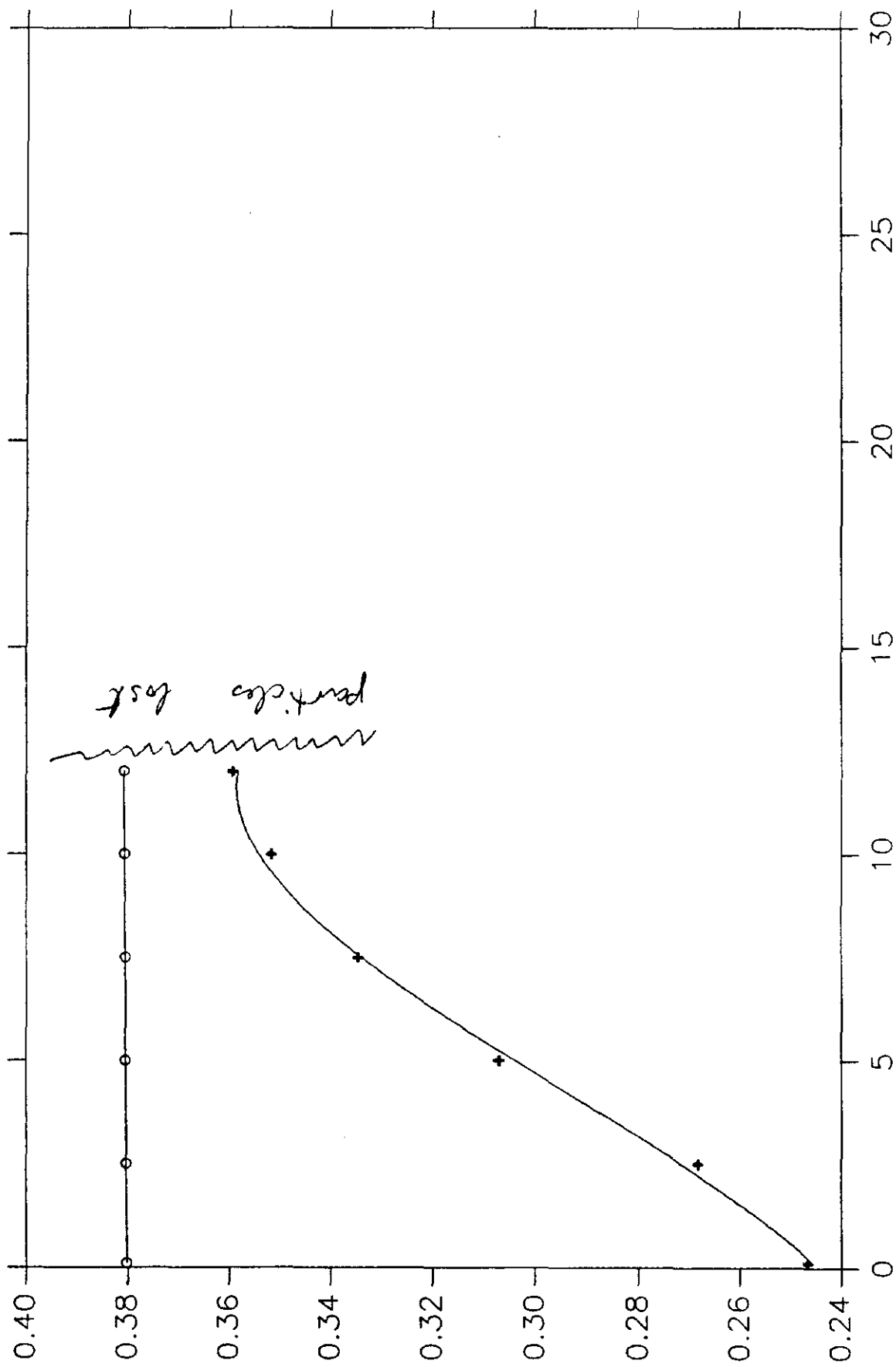
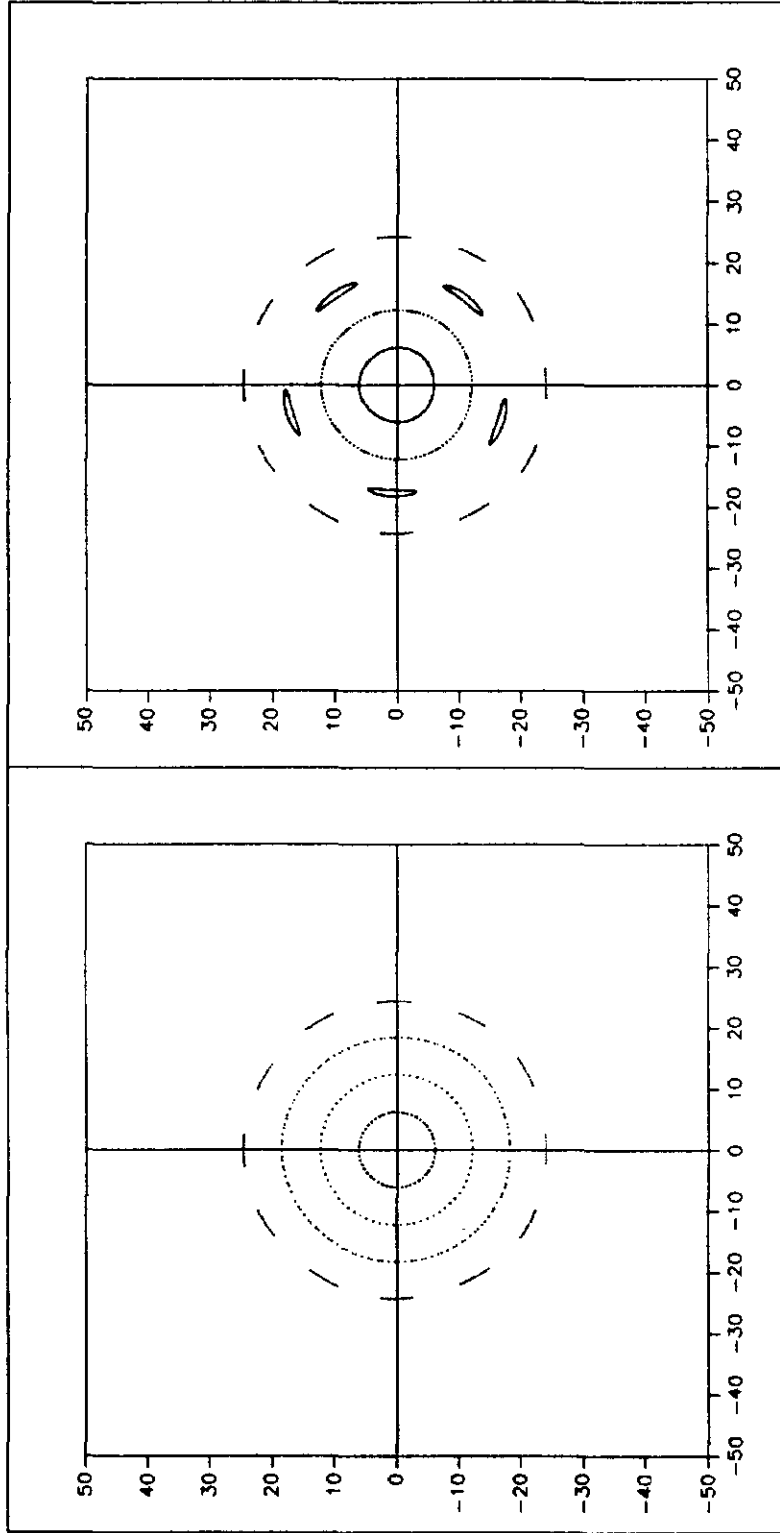


Fig 10

(b)



(a)

Fig 11

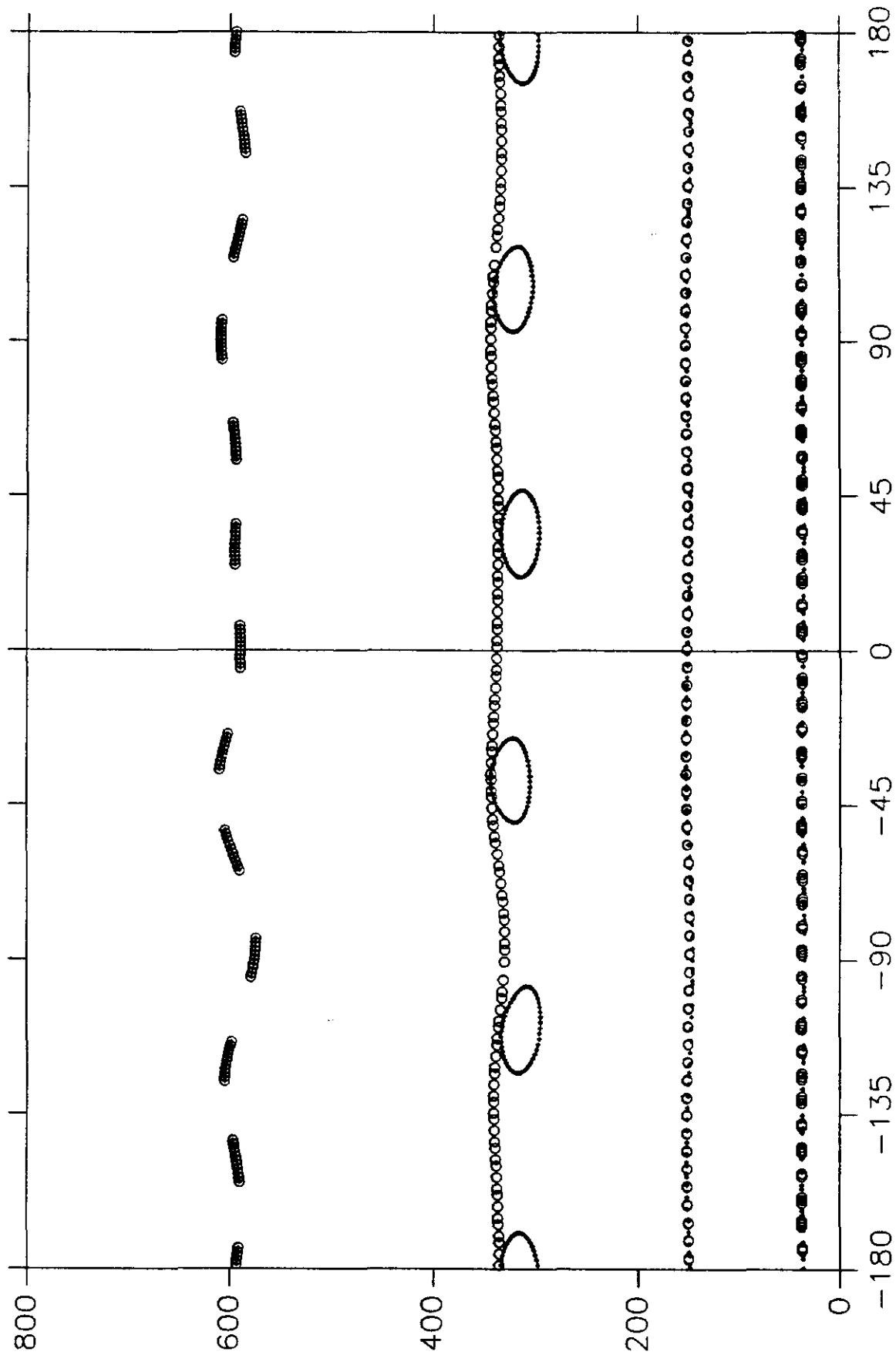


Fig 12

